Brain activity modeling in general anesthesia: Enhancing local mean-field models using a slow adaptive firing rate

B. Molaee-Ardekani,[1,2,3,*] L. Senhadji,[1,2,†] M. B. Shamsollahi,[3,‡] B. Vosoughi-Vahdat,[3] and E. Wodey[1,2,4]
[1]*INSERM, U 642, Rennes F-35000, France*
[2]*Université de Rennes 1, LTSI, Rennes F-35000, France*
[3]*BiSIPL, School of Electrical Engineering, Sharif University of Technology, Tehran, Iran*
[4]*CHU de Rennes, Service d'Anesthésie Réanimation 2, Rennes F-35000, France*
(Received 12 October 2006; revised manuscript received 26 April 2007; published 19 October 2007)

In this paper, an enhanced local mean-field model that is suitable for simulating the electroencephalogram (EEG) in different depths of anesthesia is presented. The main building elements of the model (e.g., excitatory and inhibitory populations) are taken from Steyn-Ross *et al.* [M. L. Steyn-Ross *et al.*, Phys. Rev. E **64**, 011917 (2001), D. A. Steyn-Ross *et al.*, Phys. Rev. E **64**, 011918 (2001)] and Bojak and Liley [I. Bojak and D. T. Liley, Phys. Rev. E **71**, 041902 (2005)] mean-field models and a new slow ionic mechanism is included in the main model. Generally, in mean-field models, some sigmoid-shape functions determine firing rates of neural populations according to their mean membrane potentials. In the enhanced model, the sigmoid function corresponding to excitatory population is redefined to be also a function of the slow ionic mechanism. This modification adapts the firing rate of neural populations to slow ionic activities of the brain. When an anesthetic drug is administered, the slow mechanism may induce neural cells to alternate between two levels of activity referred to as up and down states. Basically, the frequency of up-down switching is in the delta band (0–4 Hz) and this is the main reason behind high amplitude, low frequency fluctuations of EEG signals in anesthesia. Our analyses show that the enhanced model may have different working states driven by anesthetic drug concentration. The model is settled in the up state in the waking period, it may switch to up and down states in moderate anesthesia while in deep anesthesia it remains in the down state.

DOI: 10.1103/PhysRevE.76.041911 PACS number(s): 87.19.La, 87.15.Aa, 87.80.Vt, 87.90.+y

I. INTRODUCTION

In the last decade, there have been many efforts to build monitors dedicated to the estimation of the depth of anesthesia using electroencephalogram (EEG) recording [1]. However, until now there is no universal monitor able to provide reliable results in all cases (i.e., drugs, patient dependencies, etc.). Better understanding of underlying neuronal mechanisms of the EEG may improve the performance of monitoring methods. Therefore, a physiological-based model that explains the evolution of the EEG signal in different depths of anesthesia may bring new insights into the monitoring of the depth of anesthesia. Mean-field (MF) models [2,3] are good candidates for this purpose. They have neurophysiological and neuroanatomical foundations and are based on the concept of neural population, which handles thousands of similar neurons in a single structure. They are able to reproduce EEG-like signals with a low computation cost by solving a set of coupled differential equations.

One of the best MF models, which can reproduce various EEG rhythms, is the Liley model [4,5]. Steyn-Ross *et al.* [6–8] and Bojak *et al.* [9] have employed the Liley model in different ways to describe how and why the dominant rhythm of the EEG changes from beta and alpha rhythms to delta rhythm by administration of anesthetic drugs. They differently express certain parameters of the Liley model as functions of anesthetic drug concentration and reproduce EEG signals in various drug concentrations. Although these models describe the reason why anesthesia slows down EEG rhythms, they have some limitations that must be addressed gradually by better understanding of brain functioning under anesthesia.

It has been shown that there is a good compatibility between fluctuations of high amplitude delta waves and internal states of cortical cells [10,11]. During anesthesia, neural cells alternate almost synchronously between firing and rest modes that are referred to as up and down states, respectively. Because of synchronization of neurons, neural populations have two different firing modes. This means that populations switch to up and down states during anesthesia. In previous MF models, it is assumed that neural populations always fluctuate about single equilibrium points.

The main purpose of this study is to show how MF models may be enhanced by including a slow modulating mechanism that is responsible for switching the state of the model to up and down. Many mechanisms have been presented as responsible mechanisms for generating the up and down states [12–14]; however, it is still unclear which mechanisms play the most important roles, and how they can be represented using the mean-field paradigm. Since we are mostly interested in introducing the general concepts of up and down states and their switching in neural populations, an enhanced MF model that integrates a generic form of a slow modulating mechanism is proposed. This mechanism acts as a representative for various types of slow ionic currents either generated in cortical or subcortical regions.

*molaee-ardekani@ieee.org
†Corresponding author; lotfi.senhadji@univ-rennes1.fr; FAX: (+33)223236917
‡mbshams@sharif.edu

In the next section, a brief state of the art of MF models in anesthesia is reported. Section III introduces the proposed enhanced model. Section IV mainly discusses methods for analyzing the enhanced model. Finally, behaviors of the enhanced MF model in various anesthetic drug concentrations are presented in Section V.

II. BASICS OF EEG MODELING IN ANESTHESIA

To our knowledge, research conducted by Steyn-Ross *et al.* was the first attempt to explain, using an MF model, why the gradual increase of anesthetic concentration produces a sudden transition between awareness and unconsciousness [6–8]. In their model, anesthetic agents prolong the decay time of γ-aminobutyric acid ($GABA_A$) receptors. Equilibrium solutions of the coupled differential equations in various drug concentrations make an S-bend with one unstable and two stable branches. According to Steyn-Ross *et al.*, when anesthetic concentration is gradually increased or decreased, the equilibrium solution of the model suddenly jumps from one stable branch to another and this can cause a sudden transition between awareness and unconsciousness. Since phase transitions make a hysteresis path, emergence and induction phases of anesthesia take place in different drug concentrations.

Steyn-Ross *et al.* indicate that their model may simulate the biphasic response. Biphasic response is a kind of transient activation depression of the EEG signal that occurs in induction and recovery phases of anesthesia [15]. Later, Bojak and Liley [9] modify the Steyn-Ross *et al.* model. They develop better formulations to describe inhibitory and excitatory postsynaptic potentials (IPSP/EPSP) in different anesthetic drug concentrations. Bojak and Liley also argue that anesthetic drugs reduce the firing rate of spontaneous action potentials in a relatively smooth dose-dependent manner and as a result, mean membrane potentials of inhibitory and excitatory populations do not change abruptly by increasing or decreasing anesthetic drug concentration. According to this statement, Bojak and Liley generate a large set of spectra and compare them to empirical EEG recordings using some classical features such as SEF_{90} (spectral edge frequency defined as the frequency below which 90% of the power in the electroencephalogram resides). The biphasic response of the Bojak and Liley model is produced differently compared to that of the Steyn-Ross *et al.* model. It takes place in the same drug concentration in induction and recovery phases (i.e., nonhysteresis path).

Our proposed enhanced MF model is mainly established on Steyn-Ross *et al.* [6] and Bojak and Liley models [9]. A slow ionic mechanism is also incorporated in the model that let us have a better justification of some neurophysiological phenomena. For example, this enhanced model may describe the reason for the appearance of two different modes of neural firing rates and high amplitude delta waves observed in moderate to deep depths of anesthesia.

Experimental observations show that anesthetic agents basically reduce the brain activity in a pulsating manner. Intracellular and extracellular recordings during administration of many kinds of anesthetic drugs show that neurons are bistable and have short periods of firing separated by silence phases. During firing phases the firing rate is more or less equal to the firing rate of neurons in waking periods [16,17]. Neural cells alternate between the firing phase (up state) and the silence phase (down state) almost synchronously. The result of this synchronous switching can be seen as high-energy slow waves. Figures 3 and 4 in [18] and Figs. 1 and 4 in [19] indicate that neural cells firing onsets correlate well with EEG slow waves. These waves are easily transferred in the brain media [20] and are recorded on the brain surface with high amplitudes. The enhanced MF model tries to take into account the above remarks by integrating a modulating slow mechanism to its basic foundation taken from the previous MF models.

In the Appendix, we have briefly introduced the basic eight differential equations of the enhanced model. They have been formed mainly by a combination of differential equations of the two previously mentioned well-known MF models. Figure 1 illustrates a schematic diagram of the enhanced model and its excitatory and inhibitory populations. The populations interact with each other by $GABA_A$ and α-amino-3-hydroxy-5-methylisoxazole–4-propionic acid (AMPA) receptors. According to the position of the indicated switch in Fig. 1, the model may be set either to basic or enhanced mode. In the enhanced mode, the static firing rate function corresponding to the excitatory population is substituted with a slow dynamic firing rate mechanism (see Sec. III C). This increases the number of coupled differential equations to nine.

III. ENHANCING MF MODELS IN ANESTHESIA

This section describes the physiological as well as the mathematical foundations of the enhanced model. Section III A introduces the relation between up and down states in single neurons and neural populations. Slow modulating mechanisms that cause neural populations to switch to up and down states are discussed in Sec. III B. Finally, the enhanced model equipped by a typical slow modulating mechanism is presented in Sec. III C.

A. Single neurons induce up/down sates in cortical networks

Experiments of Destexhe *et al.* and Steriade *et al.* indicate that the mean histogram of neural cells membrane potentials has two distinct peaks during anesthesia or nonrapid eye movement (REM) sleep. One of them is centered in resting potential (e.g., −70 mV) and the other one in a higher potential (e.g., −57 mV) [11,21,22]. Existence of these two peaks on the histogram is an indication of two different states in neural cells.

Based on Fujisawa experiments [23], neural cells may have different patterns of firing, each one referred to as an internal state of neural cells. Fujisawa indicates that single neurons possess some internal firing states which are coherent in adjacent neurons. He declares that an internal state of single cells in a network represent the state of the network.

Destexhe *et al.* and Steriade *et al.* indicate that single

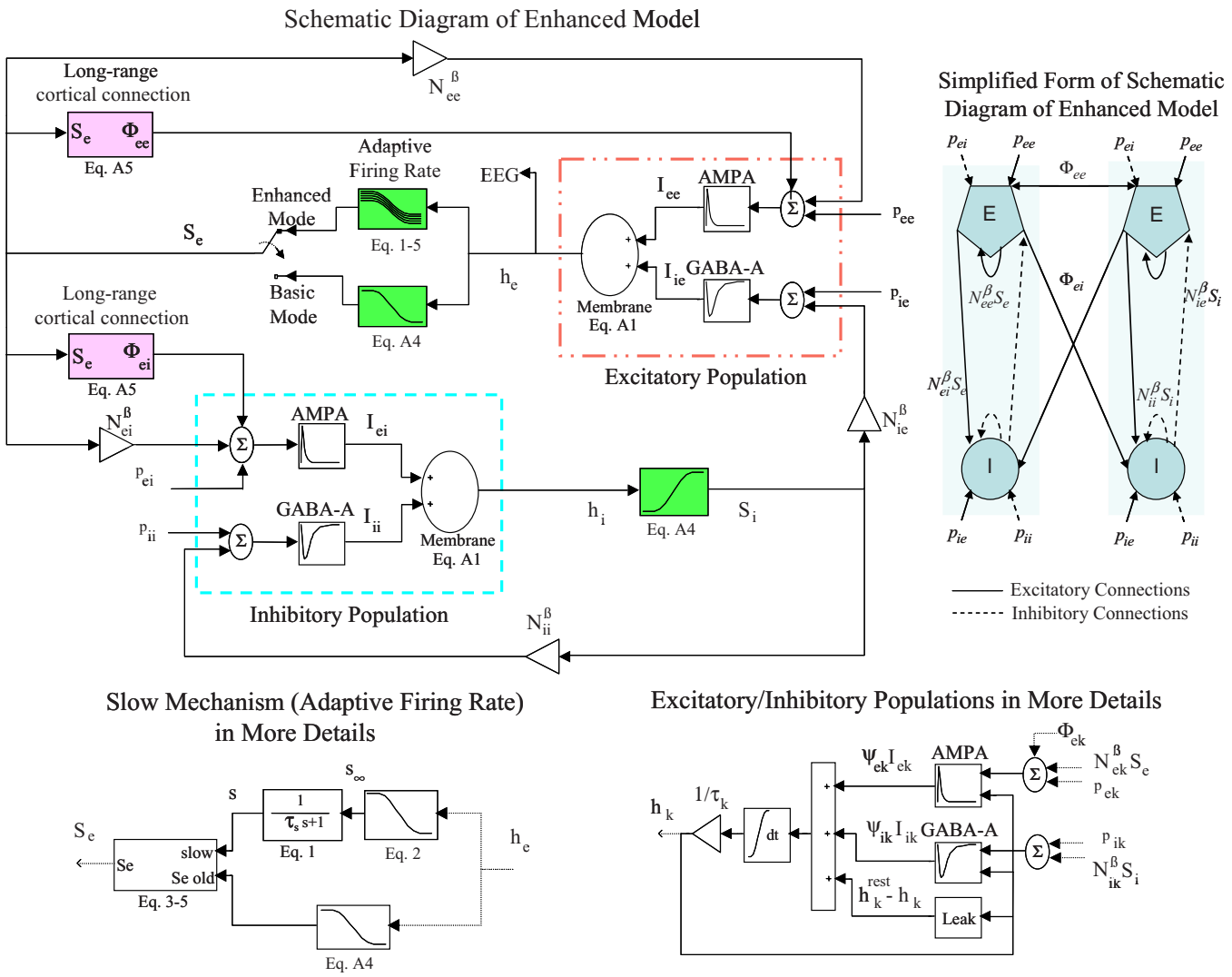

FIG. 1. (Color online) Schematic diagram of the enhanced model. The enhanced model considers the brain as a homogenous media without any kind of specialized subcortical areas. Subcortical activities are modeled by four white noises $(p_{jk}|j,k\in\{e,i\})$ that drive the excitatory (pyramidal) and inhibitory (interneurons) populations in the neocortex. Mean membrane potential of each population (h_k) is determined by inhibitory and excitatory postsynaptic potentials (I_{jk}) generated by $GABA_A$ and AMPA receptors. The model in its basic mode (see the Appendix) incorporates two sigmoid functions for determining mean firing rates of populations (S_k) from their mean membrane potentials. In addition to short-range influences of neural firing rates on $GABA_A$ and AMPA receptors, the excitatory firing rate has also long-range influences on pyramidal and interneurons by the means of AMPA receptor. In the enhanced mode, the static sigmoid function corresponding to the excitatory population is substituted by a slow dynamic equation. A more detailed block diagram related to the slow dynamic equation (see Sec. III C) and excitatory (inhibitory) populations (see the Appendix) have been illustrated in the bottom of the figure.

neurons are in two different states (up and down) and Fujisawa shows that single neurons induce phase transitions of cortical networks with multiple internal states. Inferring from these works, the neural populations have also two states of electrical activities in anesthesia or non-REM sleep and it is one of the multiple internal states of neural populations. Comparisons of the pattern of neural firings in waking and anesthesia periods show that neurons change their internal states from continuous firing to phasic firing (bursts or spikes separated by silence phases) [10,11]. Since phasic firing is almost synchronous in neural cells, the frequency of bursts or spike appearances in single neurons determines the frequency of local field potentials.

The Liley MF model [5] has the capability of generating up and down states. For instance, the upper S-bend equilibrium branch of the Steyn-Ross *et al.* model [6] can be related to up state because on the upper branch, populations have constantly high synaptic conductance and firing rates [21]. On the other hand, the lower S-bend equilibrium branch can be related to the down state. Establishing such relationships can justify the difference between synaptic conductance in the up and down states. It also describes the reason for recording of high amplitude EEG delta rhythm on brain surface during anesthesia. It seems likely that previous MF models encounter an inherent limitation in generating the slow and delta waves because they only consider either up or

down state of neural populations in various anesthetic drug concentrations.

B. Needs to insert slow ionic mechanisms in MF models

As mentioned before, neurons have two different firing states in anesthesia. Synaptic receptors and ion channels have different responses during each of these two firing states; therefore it is not only because of synaptic receptors that neural populations demonstrate two different firing states. A co-working between synapses and ionic mechanisms is responsible for generating up and down states. Neural firing patterns under different anesthetic drugs are quite different [24] and it is mainly because of unique influences that each anesthetic drug has on synaptic [25–27] or ionic [28–31] mechanisms. As a result, simulating the effects of different anesthetic drugs on EEG signals is possible if ionic currents are also considered in MF models.

Different ionic mechanisms have been hypothesized for the slow switching of neural activities to up and down states. Compte *et al.* [12] assert that the existence of slow Na^+-dependent K^+ channels (I_{KNa}) on pyramidal cells (excitatory population) is mainly responsible for pulling down the state of neurons. Massimini and Amzica [13] state that during up state the gradual reduction of extracellular Ca^{2+} concentration in response to high activity of synapses, or opening a kind of specific Ca^{2+} channel can produce a global dysfacilitation in cortical network that led it to down state. Bazhenov *et al.* [14] suggest that progressive depression of excitatory interconnections and activation of Ca^{2+}-dependent K^+ currents eventually terminate neural firing. Compte *et al.* and Bazhenov *et al.* have the same opinion in transitions of neural populations from down to up state. They declare that random summations of miniature EPSPs in some neocortex pyramidal cells are responsible for the switching from down to up state. They assert summations of miniature EPSPs activate persistent Na^+ currents ($I_{Na(p)}$) and generate action potentials. Massimini *et al.* suggest when neurons become hyperpolarized, extracellular Ca^{2+} concentration is increased linearly and dysfacilitation is removed from the network until neurons resume their firing in up state.

According to Timofeev *et al.* experiments, the slow oscillation is cortical in origin. In a decorticated brain or in a desynchronized cortex, this activity cannot be observed on thalamus and striatum [32,33], whereas it can be recorded on a deafferented cortex [34]. All aforementioned cortical ionic mechanisms have been introduced as possibly responsible mechanisms for generating the slow oscillation in the brain. However, it should be remembered that other kinds of slow mechanisms may also interfere with ionic mechanisms in the cortex. For example, intrinsic properties of thalamocortical cells (i.e., I_h and I_t ionic currents) generate a stereotype delta oscillation [35]. However, it should be noticed that they cannot be reflected at the macroscopic level of the EEG unless thalamic neurons are synchronized by slow oscillations originated from cortical regions [36]. It is also not so clear yet whether EEG delta oscillations basically come from thalamocortical stereotype oscillations or from waves generated in the cortex.

Instead of engaging with various kinds of slow ionic mechanisms in cortical and subcortical regions, in this paper we propose to formulate their overall characteristics and effects by a generic slow ionic mechanism. This mechanism mainly originates from intrinsic ionic currents of neural cells and it can be represented by a single or coupled slow gating variable. Gating variables should activate (inactivate) an inward (outward) current in down state or activate (inactivate) an outward (inward) current in up state.

It should be emphasized that it is not possible to insert neuronal-level equations of slow gating variables directly in MF models. In fact, gating variables are intrinsic properties of single neurons. For example, an ionic current, which is activated in a high voltage by a burst of action potential, would not be activated if it is included in a MF model as it is employed in a single neuron. Their counterparts need to be defined in the context of MF models.

C. Modeling slow ionic mechanisms in MF models

We can roughly formulate the activation or inactivation of slow ionic mechanisms or facilitation and dysfacilitation of neurons in a MF model by a slow variable s. Here, we assume that the variable s slowly follows $s_\infty(h_e)$ (an instantly voltage-dependent variable) according to Eq. (1). $s_\infty(h_e)$ is the activity of the slow mechanism when the membrane potential is kept constant. The slow mechanism is activated in low potentials so $s_\infty(h_e)$ is represented by a descending sigmoid function.

$$\tau_s \frac{d}{dt} s(t) = s_\infty - s(t), \tag{1}$$

$$s_\infty = s_\infty^{\max} / \{1 + \exp[-g_s(h_e - \theta_s)]\}, \quad g_s < 0. \tag{2}$$

τ_s is the time constant, $s_\infty^{\max}$ is the maximum value of the sigmoid function, θ_s is the inflection point of the sigmoid function, and g_s is the slope at the inflection point.

Equations (1) and (2) show how the membrane potential can influence the activity of the slow mechanism. On the other hand, the slow mechanism is able to modulate the firing rate of neural populations. In the enhanced model, the modulating effect of the slow mechanism is applied on excitatory population. Modulating the excitatory firing rate has indirect effects on other parameters of the model such as excitatory and inhibitory membrane potentials. An increase of s in an up or down state increases the firing rate of neural populations. In the down state, an increase of s is equivalent to the removal of dysfacilitation and an increase of miniature EPSPs. In the up state, a decrease of s is equivalent to a gradual decrease of firing rate and membrane potential. Equation (3) shows how the excitatory firing rate is modulated by s. In this equation, the previously defined excitatory firing rate in Eq. (A4) was renamed $S_e^{\text{prev}}(h_e)$.

$$S_e(h_e) = [F_1(s) S_e^{\text{prev}}(h_e) + F_2(s) S_e^{\text{mod}}] / [F_1(s) + F_2(s)], \tag{3}$$

where

$$F_1(s) = a(1 - B) / \{1 + \exp[-g_F(s - \theta_F)]\} + b_1, \tag{4}$$

$$F_2(s) = aB/\{1 + \exp[g_F(s - \theta_F)]\} + b_2. \quad (5)$$

Equation (3) gathers two different terms of firing rates: $S_e^{\text{prev}}(h_e)$ and a constant modulating firing rate value S_e^{mod}. The normalized combination of these two terms determines the overall firing rate of the excitatory population. Weighting functions $F_1(s)$ and $F_2(s)$ are antisymmetric sigmoid functions. B is a free parameter that determines the gain of the modulating term S_e^{mod} by changing the balance between $F_1(s)$ and $F_2(s)$. θ_F and g_F determine the inflection point and slope of the sigmoid functions, respectively. g_F is a negative value so $F_1(s)$ and $F_2(s)$ are descending and ascending functions, respectively. b_1 and b_2 are two constant values such that set $F_1(0)$ and $F_2(0)$ to one and zero, respectively. θ_F determines the convexity of $F_1(s)$ and $F_2(s)$ functions over the interval $[0, s_\infty^{\max}]$. Since $F_1(s)$ and $F_2(s)$ are fixed to one and zero, respectively, at zero, θ_F and g_F may influence the values of these two functions at $s_\infty^{\max}$. Parameter a compensates this effect and force $F_1(s)$ and $F_2(s)$ to have the same value at $s_\infty^{\max}$ for a given B regardless of the values of θ_F and g_F. We have chosen $\theta_F = 0.1$, $g_F = -3.5$ as our references for normalization of these functions. If θ_F and g_F are equal to 0.1 and -3.5, respectively, a would be equal to one. In brief, a, b_1, and b_2 are obtained as follows:

$$a = \frac{\{1 + \exp[g_F(s_\infty^{\max} - \theta_F)]\}[1 + \exp(-\theta_F g_F)][1 - \exp(-3.5 s_\infty^{\max})]\exp(3.5 \times 0.1)}{\{1 + \exp[3.5(0.1 - s_\infty^{\max})]\}[1 + \exp(0.1 \times 3.5)][1 - \exp(g_F s_\infty^{\max})]\exp(-g_F \theta_F)}, \quad (6)$$

$$b_1 = 1 - a(1 - B)/\{1 + \exp(g_F \theta_F)\}, \quad (7)$$

$$b_2 = -aB/\{1 + \exp(-g_F \theta_F)\}. \quad (8)$$

Figure 2 illustrates $F_1(s)$ and $F_2(s)$ for some different values of θ_F and g_F. For each coupled θ_F and g_F values, b_1, b_2, and a are tuned so that boundaries of $F_1(s)$ and $F_2(s)$ do not change for the same given gain of modulating mechanism B.

To study influences of s, θ_F, and B on the excitatory firing rate, some samples of these variables (e.g., $\{0, 0.33, 0.66, 1\}$, $\{0.1, 0.9\}$, and $\{0.16, 0.04\}$, respectively) are selected and their corresponding excitatory firing rates are sketched in Fig. 3. Increasing the s value raises the excitatory firing rate. Activation of the slow mechanism s has more influence on the increase of the firing rate in low potentials. This is mainly due to the generation of spikes or bursts in low membrane potentials when slow modulating mechanisms are activated. A comparison of the left and right graphs in Fig. 3 show that B magnifies the influence of s on the firing rate. B does not change excitatory firing rate values corresponding to $s = 0$. By comparing the graphs in the top and bottom it can be understood that θ_F may change the ascending patterns of sigmoid functions. However, it does not change the boundary values of the excitatory firing rates. In another word, it does not change excitatory firing rate values corresponding to $s = 0$ and $s = s_\infty^{\max}$ as was shown in Fig. 2.

Anesthetic concentration affects amplitudes and decay times of EPSPs and IPSPs as well as the activity of the slow mechanism. For instance, it has been shown that anesthetic drugs in very high concentrations may reduce inward currents [30,31]. In order to take into account such a phenomenon we can reduce the maximum activity of the slow mechanism by reducing B or θ_s values when anesthetic concentration is increased.

IV. MODEL SOLUTIONS

A general way to examine the behavior of the variables of the model $(h_k, I_{jk}, \Phi_{ek}, s, \dot{I}_{jk}, \dot{\Phi}_{ek} | j, k = \{e, i\})$ is to obtain the numerical solution of the coupled differential equations. If the variables exhibit stable behaviors, generally a good compatibility exists between power spectrums calculated by numerical and analytical methods. Otherwise, when the variables do not converge to equilibrium points, it is not possible to use analytical methods to evaluate their behaviors. Although in such a case numerical solution is employed to examine the behavior of the variables, investigations of equilibrium solutions, isoclines, and their corresponding vector field may give insight into the behavior of the variables before deriving the numerical solution.

This section is divided into two parts. In the first part, a numerical solution of the enhanced model is described. Equilibrium solutions of the model, isoclines, and their corresponding vector field are mainly described in the second part.

A. Numerical solution of the model

The nine coupled differential equations of the model consist of three first-order and six second-order equations (four of them are stochastic differential equations). Second-order differential equations can be substituted by pairs of first-order differential equations. The general form of the resulting first-order differential equations and their corresponding first-order difference equations are

$$\frac{d}{dt}x(t) = F(h_e(t), h_i(t)) + A\xi(t), \quad (9)$$

$$x[n+1] = (x[n] + F(h_e[n], h_i[n]))\Delta t + A\sqrt{\Delta t}\xi[n], \quad (10)$$

where n is the discrete time, $\xi[n]$ is a zero mean uniform white noise with $\frac{4}{12}$ variance [see Eq. (A6)] and Δt is the

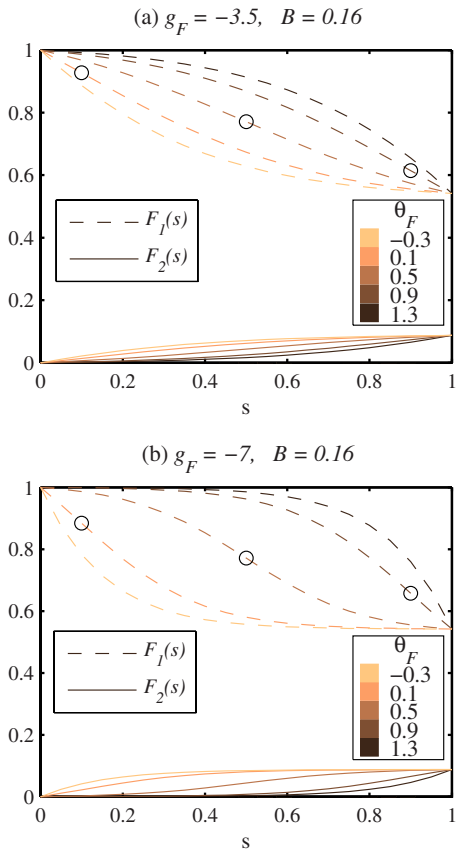

FIG. 2. (Color online) Influences of θ_F and g_F on weighting functions $F_1(s)$ and $F_2(s)$. These two functions determine the firing rate of excitatory population based on two competing terms $S_e^{\text{prev}}(h_e)$ and S_e^{mod}. An increment of s raises the firing rate by increasing (decreasing) the value of $F_2(s)/F_1(s)$. θ_F determines their convexities. If θ_F is smaller than zero, $F_1(s)$ and $F_2(s)$ are convex and concave functions, respectively, in the range of zero and $s^{\max}$. Convexities are reversed if θ_F is greater than $s^{\max}$. In between, these two functions have inflection points that are indicated on $F_1(s)$ by circles. g_F controls slopes of $F_1(s)$ and $F_2(s)$.

time increment value (step size) in the Euler method, and it was set to 1 ms in our simulations. We could not see any significant changes in numerical results when we used smaller time steps such as 0.1 or 0.01 ms.

Basically, the main purpose of performing the numerical simulation of the model is to find the time evolution of $h_e(t)$ and $s(t)$ (better to say $h_e[n]$ and $s[n]$) for different anesthetic drug concentrations. In order to do so, drug effects are first applied to IPSP and EPSP parameters (or any other desired parameter such as the slow mechanism) according to Eqs. (A7) and (A8). In the next step, the numerical values of the variables of the model are calculated by the Euler one-step scheme for 51.2 s. In the Euler method, the initial values of the variables are set to their equilibrium values. The simulated signals are down sampled to 400 Hz in order to be comparable with our real EEG recordings on children [37]. Table I lists the numerical values and definitions for the equation parameters and constants. These numerical values are used throughout this paper, except where stated otherwise.

B. Equilibrium solution, isoclines, and vector field

Equilibrium solution of the model provides much information about the functioning mode of the model. For example, the equilibrium value of $h_e(t)$ may provide some information about the balance between excitatory and inhibitory populations, and the status of the patient such as waking, light, or deep anesthesia.

As mentioned before, isoclines may be helpful when the variables of the model do not converge to equilibrium points. To obtain p isoclines in a p-dimensional (pD) hyperplane, p variables are first selected from the entire m variables of the model, then the equilibrium solution of each variable is calculated while maintaining others to different constant values. The trajectory of the p variables can be sketched in a pD space, but predicting the new position of the trajectory requires obtaining an mD vector field. Directions and lengths of the vectors in this field determine the dynamics of the trajectory. If $p=m$, the vector field can be sketched in the pD space.

By some simplifying assumptions it is possible to reduce the value of m. For example, we can assume that all variables are fast enough compared to h_e, h_i, and s to have a simplified model that only consists of three dynamic variables. Since we are mainly interested in evaluating the role of slow variable s on the EEG signal, we derive $dh_e/dt=0$ and $ds/dt=0$ isoclines (called s,h_e isoclines) in Sec. IV B 1. The corresponding vector field of s,h_e isoclines is a three-dimensional (3D) vector field that cannot be sketched in a plane. In Sec. IV B 2, we propose a method that reduces the 3D vector field to a planar vector field. It should be remembered that the 3D simplified model is only used to obtain the planar vector field. Numerically simulated signals and their corresponding trajectories (in Sec. V) are derived from the full model.

1. Isoclines of the slow mechanism and excitatory membrane potential

One of the best ways to study the influence of slow variable s on the model behavior in different anesthetic concentrations is to sketch s, h_e isoclines and the trajectory of $s(t)$ and $h_e(t)$ signals in the same plane. If ds/dt is set to zero in Eq. (1) and h_e is calculated as a function of s, the result will be $ds/dt=0$ isocline (simply called s isocline). On the other hand, declaring s as a function of h_e when $dh_e/dt=0$ in Eq. (A1) results in h_e isocline. It should be remembered since we only obtain two isoclines of the simplified model, h_i must be set to its equilibrium value in Eq. (A1). In this case, a simple method to calculate h_e isocline is to vary s between zero and $s_\infty^{\max}$ with a definite step size (e.g., 0.05) and compute the equilibrium values of h_e and h_i in parallel (they are referred to as $h_e^\bullet$ and $h_i^\bullet$).

Figure 4 shows two typical superimposed s,h_e isoclines. Intersections of these two isoclines determine the equilibrium solutions of the differential equations ($ds/dt=dh_e/dt=0$). Any other point on the isoclines plane may have positive or negative values of ds/dt and dh_e/dt. These values can be represented by a vector field. Length and direction of any given member vector of this vector field show how s and h_e

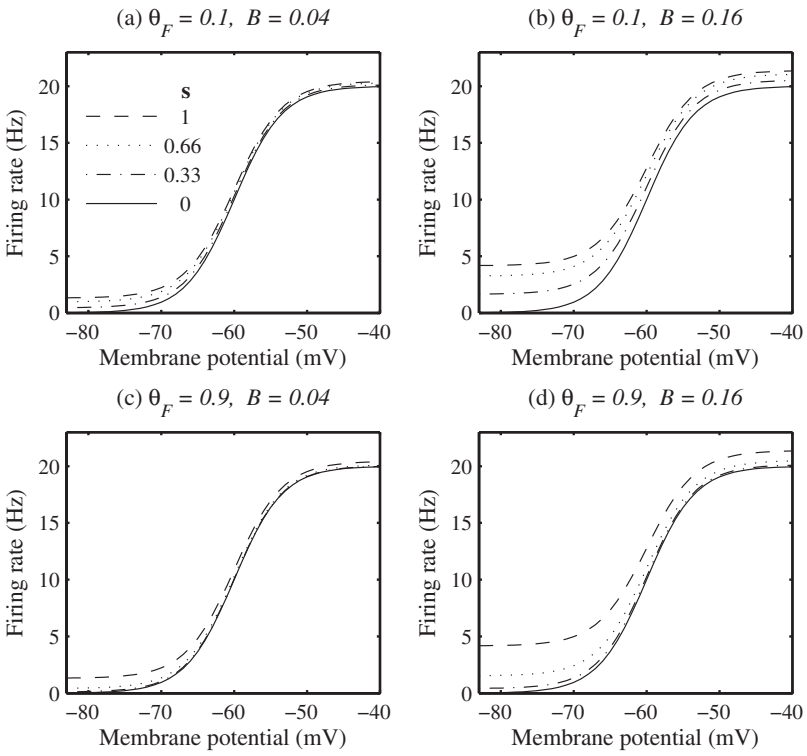

FIG. 3. Influences of s, θ_F, and B on the excitatory firing rate. An increase of s raises the firing rate value especially in low membrane potentials. Increasing the gain of the modulating mechanism B from 0.04 to 0.16 (compare left and right figures) increases the influence of s on the excitatory firing rate. θ_F does not change the value of the excitatory firing rates at boundaries of s (i.e., at 0 and $s_\infty^{\max}$) but it can affect the ascending shape of the excitatory firing rates corresponding to $0<s<s_\infty^{\max}$ (compare top and bottom figures).

vary if the state of the model is located on the origin of that vector.

2. Obtaining planar vector field on isoclines plane

In Fig. 4, in addition to s,h_e isoclines (dashed line and solid line with hexagram marks) we have also shown nine member vectors of a planar vector field in ($s=0.4$, $h_e=h_e^\bullet+\Delta h_e$), where $\Delta h_e=\{-1,0,1\}$ mV and $h_e^\bullet$'s are red hexagram marks on h_e isocline. Ordinates and abscissas of the vectors are proportional to ds/dt and dh_e/dt, respectively. ds/dt is simply calculated from Eq. (1), but obtaining dh_e/dt from Eq. (A1) requires more considerations. A glance into Eq. (A1) reveals that in addition to h_e, h_i also influences the value of dh_e/dt. As a result, since h_i is a dynamic variable in the simplified model, a 3D vector field $(dh_e/dt, dh_i/dt, ds/dt)$ is associated to the model.

To find a planar vector field that can be used instead of the 3D vector field, variable h_i should be replaced by a static value. In order to do so, we examined different planar vectors in different points around h_e isocline [i.e., $(s,h_e^\bullet+\Delta h_e)$]. In each given point, planar vectors were different in their abscissas (i.e., dh_e/dt) because of the various h_i values that were used in Eq. (A1). These values were confined to $h_i^\bullet+\Delta h_i$ values, where $\Delta h_i=\{\pm 1.4, \pm 1.2, \ldots, \pm 0.2, 0\}$. We observed visually that lengths and directions of vectors for which $\Delta h_i \simeq D/(h_e^\bullet-h_i^\bullet+D)$, $D=5$ mV, fit well trajectories. As a result, these planar vectors are good candidates to be used instead of 3D vectors. Although these vectors are obtained roughly by this method, it is possible to track simulated signals by a planar vector field $(dh_e/dt, ds/dt)$. This approximation can be used as a useful method for tuning the model parameters and balancing the excitatory and inhibitory factors. It is important to remember that s,h_e isoclines and their corresponding planar vector field cannot describe the whole dynamics of the model. For example, other variables may start limit cycles that are unpredictable by s,h_e isoclines; therefore, a numerical solution may still be necessary to confirm results provided by isoclines.

V. BEHAVIOR OF ENHANCED MF MODEL IN VARIOUS DRUG CONCENTRATIONS

In this section, we study the evolution of the EEG signal during various anesthetic concentrations. We perform several numerical simulations in different drug concentrations (from low to high) and describe characteristics and morphologies of the simulated EEG signals. In order to compare the reproduced EEG signals with empirical data, we bring some real EEG signals recorded on children undergoing surgery with Desflurane agent (see [37] to see the protocol of EEG recording). In Desflurane anesthesia, 1 minimum alveolar concentration (MAC) is equivalent to applying 8.3 vol % of this gas to children [38]. This value corresponds to $c \simeq 0.73$ mM aqueous concentrations of Desflurane in saline [39,40].

A. Waking and sedation

In the enhanced model, s,h_e isoclines obtained in waking situation are very similar to those derived for a very low anesthetic drug concentration. Figure 5(a) shows a 10 s (s,h_e) trajectory superimposed on s,h_e isoclines in $c=0.2$ mM. Figure 6(a) illustrates that part of the $h_e(t)$ which forms the depicted trajectory in Fig. 5(a). The power spectrum of $h_e(t)$ is shown in Fig. 7(a) (solid line). In Fig. 5(a), coordinates of the intersection point of the two isoclines in-

TABLE I. Symbol definitions and constants values of the enhanced model.

Parameter	Symbol	Value
Mean resting membrane potential	$h_{e,i}^{\text{rest}}$	−77, −77 mV
Passive membrane decay time constant	$\tau_{e,i}$	45, 30 ms
Synaptic reversal potential	$h_{e,i}^{\text{rev}}$	0, −85 mV
Peak amplitude of EPSP/IPSP	$G_{e,i}$	0.3, 0.32 mV
EPSP/IPSP rate constant	$\gamma_{e,i}$	0.5, 0.15 ms^{-1}
Total number of $e\rightarrow e$, $e\rightarrow i$ local synaptic connections	$N_{ee,ei}^{\beta}$	2400, 2300
Total number of $i\rightarrow e$, $i\rightarrow i$ local synaptic connections	$N_{ie,ii}^{\beta}$	200, 440
Total number of synaptic connection from distant excitatory population	$N_{ee,ei}^{\alpha}$	2000,1600
Spatial drop-off rate of long-range excitatory connections	Λ	0.4 cm^{-1}
Mean axonal conduction speed	$\bar{v}$	0.7 cm ms^{-1}
Maximum firing rate	$S_{e,i}^{\max}$	0.02, 0.02 ms^{-1}
Inflexion-point voltage for firing rate sigmoid function	$\theta_{e,i}$	−60, −60 mV
Firing rate sigmoid slope at inflexion point	$g_{e,i}$	0.3, 0.3 mV^{-1}
Subcortical mean firing rate	$\bar{p}_{ek},\bar{p}_{ik}$	0.5, 0.4 ms^{-1}
Weighting factors for fluctuations in $\bar{p}_{jk}$ spike inputs	α	1
Effective time constant of slow ionic currents	τ_s	180 ms
Slope at the inflexion point of the activity function (sigmoid) of slow mechanism	g_s	−0.8 mV^{-1}
Inflexion-point voltage of the activity function (sigmoid) of slow mechanism	θ_s	−58.8 mV
Maximum value of the activity function (sigmoid) of slow mechanism	$s_{\infty}^{\max}$	1
Slope at the inflexion point of the modulating sigmoid function	g_F	−3.5
Inflexion point of the modulating sigmoid function	θ_F	0.1
Maximum firing rate due to the modulating mechanism.	S_e^{mod}	0.03 ms^{-1}
Gain of the modulating mechanism	B	0.16

dicate the equilibrium values of $s(t)$ and $h_e(t)$ signals. The intersection point is located somewhere in the up state area. Head to head directions of the vectors about this equilibrium point indicate that it is a stable equilibrium point. The histogram of $h_e(t)$ in Fig. 8(a) also shows that the equilibrium point is stable because h_e fluctuations are centered about a fixed point in the up state area. These fluctuations are actually the result of the asynchronous firing mode in neural cells. In such a case, the balance between excitatory and inhibitory populations is the most important factor in determining the characteristics of inhibitory and excitatory membrane potentials and firing rates [41]. This balance is mainly determined by (i) subcortical noises that are modeled by white uniform noises (p_{jk}), (ii) characteristics of IPSPs and EPSPs, and (iii) connectivity properties of the two populations. In fact, these factors determine a particular model operating state (equilibrium solution) and thus the characteristics of h_e fluctuations. It is straightforward to derive the eigenspectrum (power spectrum) of h_e by taking Fourier transform of the linearized form of the coupled differential equations about their equilibrium values. Figure 7(a) illustrates the analytically calculated eigenspectrum of h_e (dashed line) when drug concentration is 0.2 mM. For comparison, a typical real EEG signal is illustrated in Fig. 9(a). This signal is recorded on a child a few seconds before administration of Desflurane agent. The power spectrum of the illustrated EEG signal in Fig. 9(a) is shown in Fig. 10(a). It should be mentioned that the patient is awake, a little agitated, and eyes are open. This situation causes the energy of the alpha band to be lower compared with the energy of the alpha band in the eyes-closed condition.

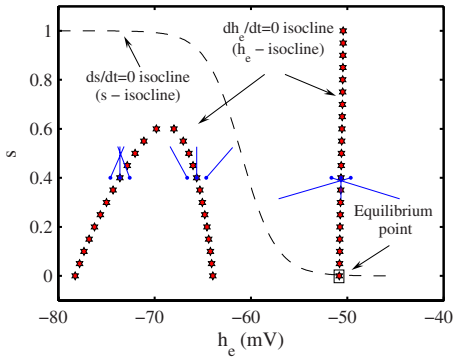

FIG. 4. (Color online) A typical s isocline (dashed line) and h_e isocline (hexagrams) and nine candidate planar vectors. Origins of the vectors are located in $(s=0.4, h_e^{\bullet}+\Delta h_e)$, where $\Delta h_e=\{-1,0,+1\}$ mV and $h_e^{\bullet}$ is the equilibrium point of the model in a given s value (blue hexagrams). The intersection point of the two isoclines (s, h_e isoclines) indicates the equilibrium point. Coordinates of this point indicate the equilibrium values of h_e and s. Convergent or divergent directions of vectors around a given point on h_e isocline determine stability or instability status of that point.

Besides focusing on intersections of isoclines and equilibrium solutions of s and h_e, assessing the behavior of the model when s takes different constant values is of interest especially in cases when the trajectory runs away from the attracting area of a stable equilibrium point or when an equilibrium point is unstable. Since h_e converges to its equilibrium value faster than s, on a short time period, s can be assumed constant and the behavior of the trajectory can be mainly thus studied by means of h_e isocline. It is important to remember that for any point on h_e isocline, dh_e/dt is equal to zero and following the fast convergence of a trajectory to h_e isocline, dh_e/dt value also converges to zero rapidly. Consequently, in an instability mode, trajectories are mainly located in the vicinity of h_e isocline, and we generally need to obtain only a few members of the planar vector field in the vicinity of h_e isocline and not over the entire isoclines plane.

In Fig. 5(a), h_e isocline shows that those equilibrium solutions corresponding to $0.25<s<1$ make a single branch in the up state area, while those corresponding to $s<0.25$ make

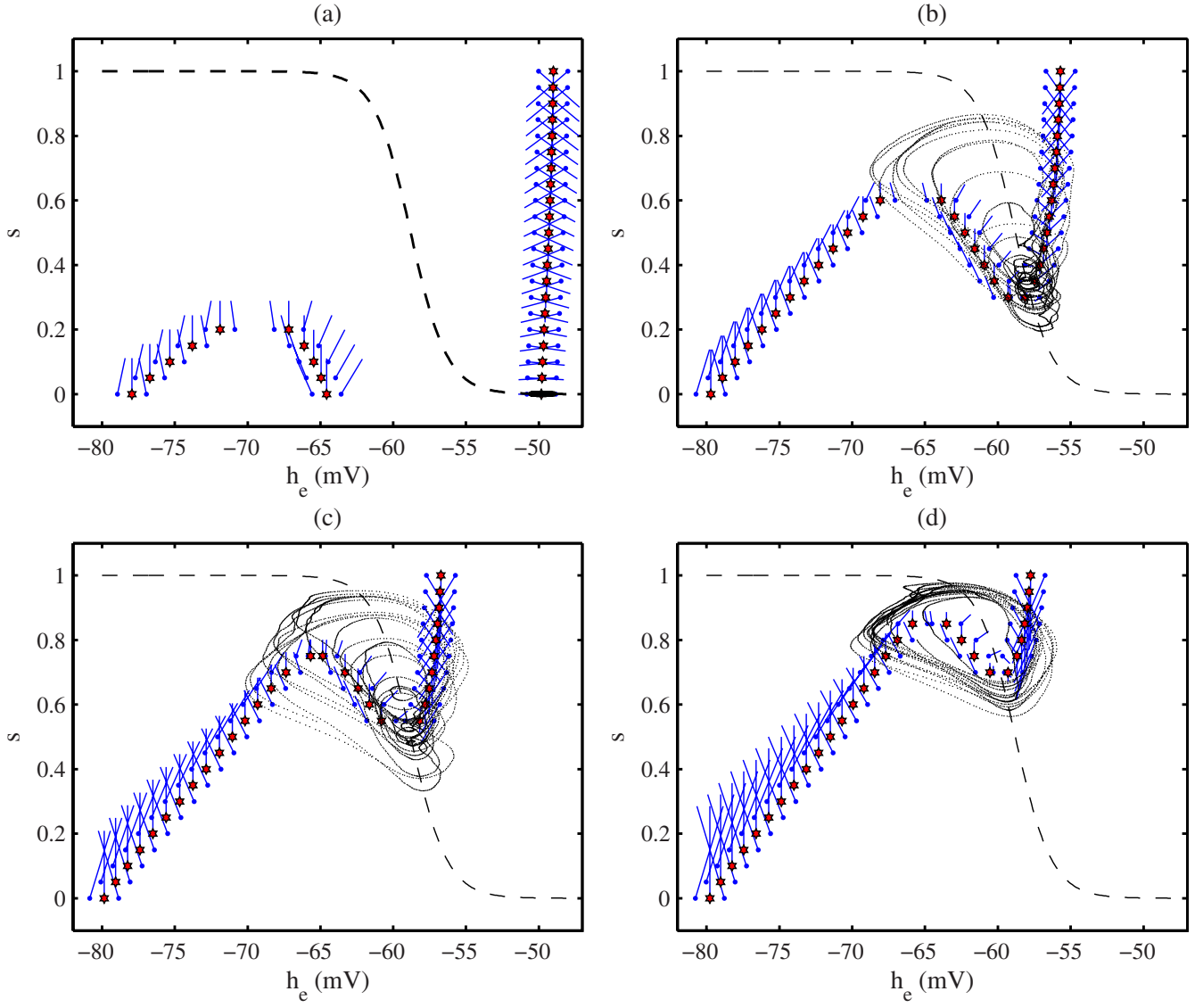

FIG. 5. (Color online) s, h_e isoclines (dashed line and hexagrams) and 10 s (s, h_e) trajectories superimposed on them in different depths of anesthesia. Ordinates and abscissas of vectors (solid lines marked at vector origins) are proportional to the values of ds/dt and dh_e/dt, respectively. (a) When drug concentration is low ($c=0.2$ mM), $h_e(t)$ fluctuates about a stable equilibrium point. (b) When drug concentration increases to 0.75 mM, slow waves appear on background noisy fluctuations. (c) In $c=0.9$ mM background noisy fluctuations are substituted with a more rhythmic activity. (d) When anesthetic concentration is set to 1.5 mM, the trajectory travels between up and down states regularly.

three branches in down, middle, and up state areas. Equilibrium points located in the middle branch are unstable. This is known from the opposite directions of planar vectors in the vicinity of these equilibrium points. The probability of finding a trajectory in the vicinity of these points is low. The up state equilibrium points have the highest probability of occurrence compared with the two other types of equilibrium points. If $h_e(t)$ is initialized to a value greater than −64 mV and then it is perturbed by, for example, an inhibitory subcortical activity, there is a high probability that $h_e(t)$ approaches again the up state area. In contrary, vectors about the down state equilibrium points indicate that there are not enough attraction forces toward these points and even if $h_e(t)$ approaches this area, it does not stay for a long time in this state and will switch back again to the up state via a saddle point.

B. Moderate anesthetic drug concentration (about 1 MAC)

When anesthetic concentration is increased to a higher value (e.g., $c=0.75$ mM) and the balance between excitatory and inhibitory populations shifts a little toward more inhibition, the power spectrum of $h_e(t)$ shifts to lower frequencies. Compared to Fig. 5(a), in Fig. 5(b) the right branch of h_e isocline has moved a little to more negative potentials and the inverse U-turn has moved to up and right sides. Since s positively modulates the excitatory firing rate in Eq. (3), movement of the inverse U-turn toward more positive s val-

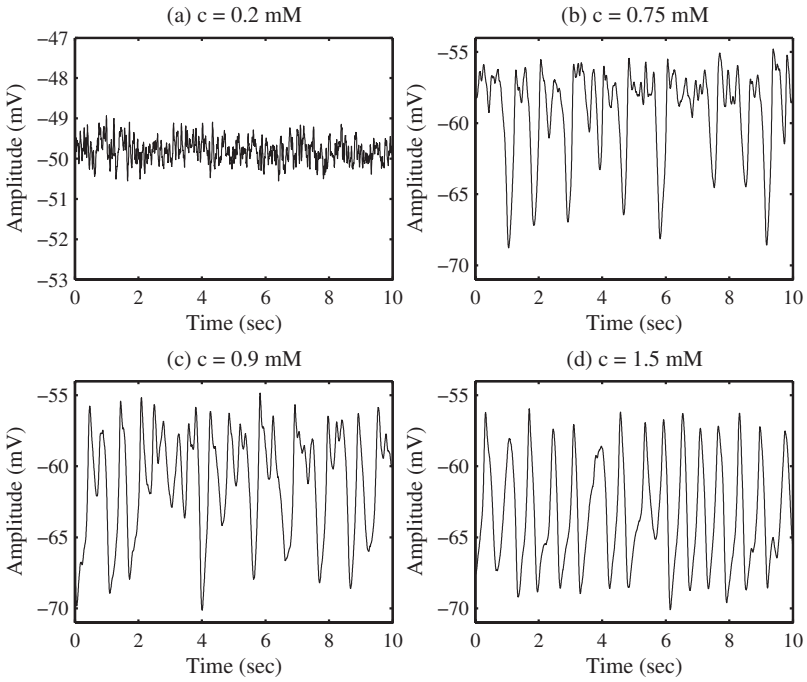

FIG. 6. Ten seconds of simulated h_e signals in various anesthetic concentrations (0.2, 0.75, 0.9, and 1.5 mM). These signals correspond to illustrated trajectories in Fig. 5.

ues indicates that the balance has moved to inhibition. As a result, for example, when s is equal to 0.4 mM three equilibrium points exist on h_e isocline depicted on Fig. 5(b), while for the same s value, only one equilibrium point can be found on h_e isocline reported on Fig. 5(a). When the distance between right and middle branches of h_e isocline is reduced, $h_e(t)$ is distributed over a wider region along the up state area so the probability of the trajectory for being in the neighborhood of the middle branch is increased. This can cause the trajectory to move along or cross the barrier of the unstable branch to reach the down state area. This is the beginning phase of slow wave episodes on the EEG signal. At first, most of the trajectory cycles encounter the attraction of the up state area and the repulsion of the middle branch so they move back to the up state area. Those who reach the down state area appear as semiperiodic high amplitude negative pulses on $h_e(t)$ illustrated in Fig. 6(b). The appearance of such negative pulses extends the histogram of the h_e signal toward negative potentials [see Fig. 8(b)], but since most of the time h_e activities are related to the up state, the histogram still contains a single peak located in the up state area. Negative pulses of $h_e(t)$ increase the overall power especially in the slow delta band (0–2 Hz). Figure 7(b) illustrates a typi-

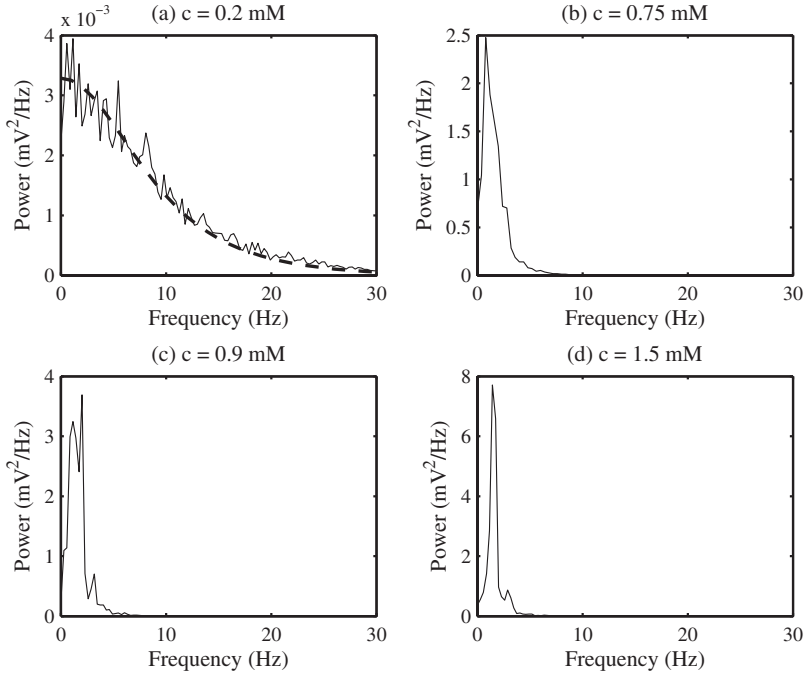

FIG. 7. The power spectra of simulated h_e signals in different drug concentrations. Each power spectrum is calculated by averaging 20 power spectra of consecutive 2.56 s h_e epochs (i.e., 51.2 s). (a) In very low drug concentration (c=0.2 mM), the power spectrum extends to high frequency terms. The eigenspectrum (dashed line) corresponding to this drug concentration is a descending function that is reminiscent of the background spectrum of a real EEG signal in the waking period. (b) Appearance of slow waves (c=0.75 mM), increases the energy of the slow delta band in the power spectrum. (c) Increasing the rate of slow waves (c=0.9 mM) increases the energy of the fast delta band in the power spectrum. (d) Regular switching between up and down state (c=1.5 mM) narrows the h_e spectrum in the fast delta band.

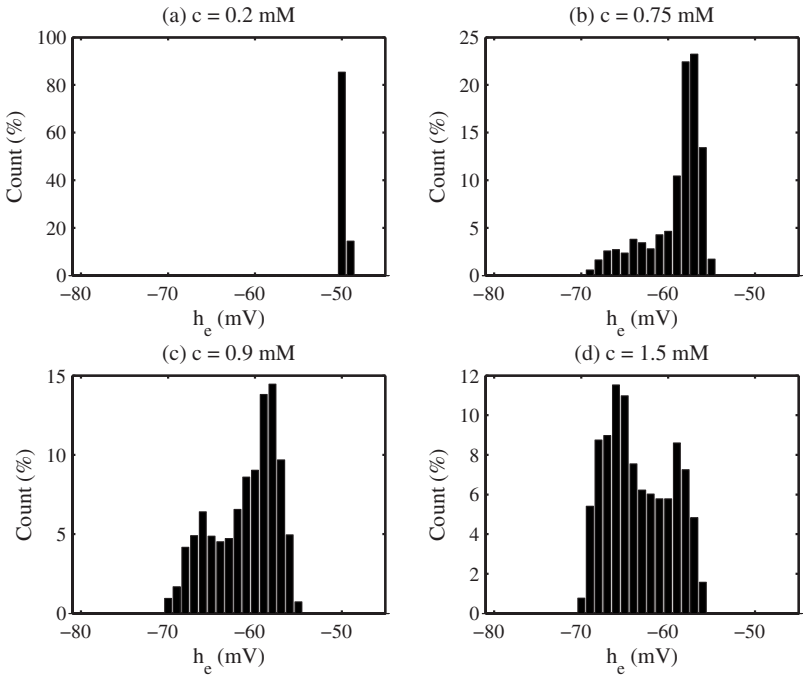

FIG. 8. Histograms of simulated h_e signals in different anesthetic drug concentrations. (a) In very low drug concentration ($c=0.2$ mM) the histogram contains only one peak centered in the up state area. (b) Slow waves extend the histogram to down state ($c=0.75$ mM). (c) The histogram contains two peaks in up and down states ($c=0.9$ mM). (d) The amplitude of the peak located in the down state may be equal or even higher than the amplitude of the other peak ($c=1.5$ mM).

cal power spectrum of $h_e(t)$ when drug concentration is 0.75 mM.

Figure 9(b) shows a typical real EEG signal recorded at 1 MAC Desflurane. A combination of high amplitude, low frequency negative peaks and low amplitude, high frequency activities is seen on the real EEG signal like what can be observed on the simulated signal in Fig. 6(b). However, it should be mentioned that amplitudes of negative slow waves on real signals may vary accidentally in successive EEG epochs. This variation may increase the standard deviation of EEG energy. It seems that interactions of different modulating mechanisms and their overall effects on the brain activity and so synchronization of neural cells in a local field may be influenced by past non-full-periodic activities of slow negative pulses. However, this is a subject that we do not deal with in this study.

Increasing the anesthetic concentration a bit more (e.g., $c=0.9$ mM), makes it possible for trajectories to jump over the barrier of the unstable area and change the state of the model from up to down easier than before. Figure 5(c) shows 10 s of (s,h_e) trajectory when c is equal to 0.9 mM [see also Figs. 6(c), 7(c), and 8(c) that show the time course, power spectrum, and histogram of $h_e(t)$, respectively]. In transition from up to down state, the value of s increases gradually

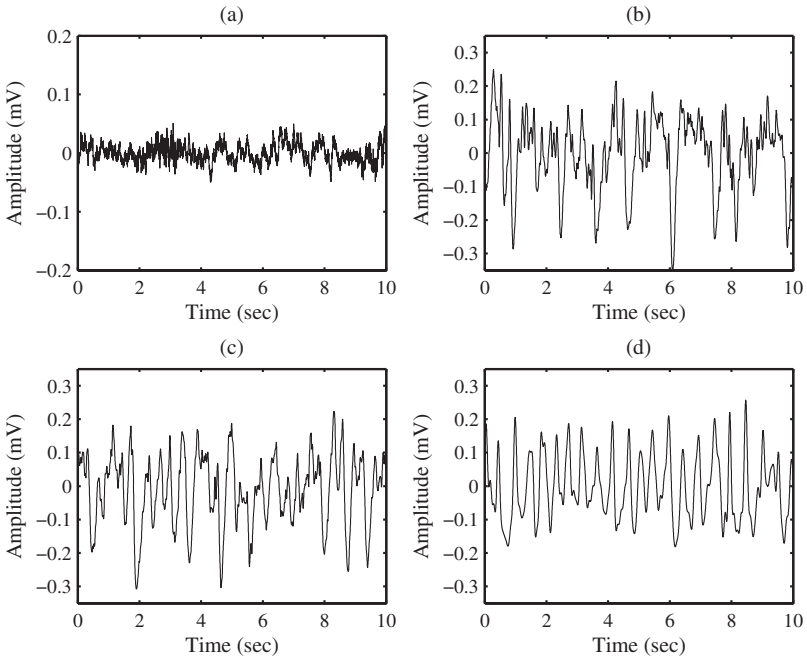

FIG. 9. Real EEG signals recorded on children undergoing surgery with Desflurane agent [37]. (a) EEG signal before administration of Desflurane. The patient is awake and in eyes-open condition. (b) EEG signal at 1 MAC anesthesia. The high amplitude negative peaks are easily distinguished from high frequency lower amplitude background EEG activities. (c) The EEG at a concentration higher than 1 MAC. The number of negative peaks is increased in this signal and high frequency, low amplitude background activities are replaced by lower frequency, higher amplitude activities. (d) EEG signal at 2 MAC. This signal mainly consists of high amplitude rhythmic pulses.

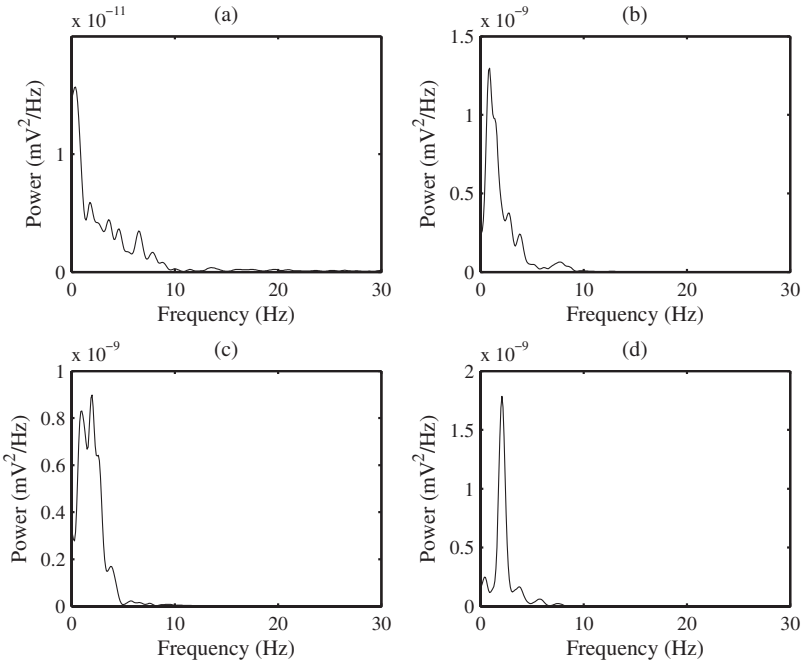

FIG. 10. Power spectrums corresponding to the illustrated real EEG signals in Fig. 9.

following the rapid change of the s_∞ value. An Increase of s continues until the trajectory approaches a saddle point (tip of the inverse U-turn). This point is the critical point where sufficient modulating factors have been accumulated in the excitatory neural population; therefore the trajectory switches back to the up state. When the switching is taking place, s is then gradually decreased until another transition from up to down state happens.

As illustrated in Fig. 6(c), the transition rate between the two states has increased compared to the case where $c=0.75$ mM. The histogram of $h_e(t)$ has now two distinct peaks that are related to down and up states, respectively [Fig. 8(c)]. But as it is shown in Fig. 5(c), the trajectory is still mainly located in the up state area and as a consequence, the amplitude of the second peak of the histogram is higher than the first one.

Figure 9(c) illustrates a real EEG signal recorded in a drug concentration that is a bit higher than 1 MAC [37]. It should be mentioned that compared to Fig. 9(b), the number of negative peaks is increased and the EEG background activity is replaced by a lower frequency, higher amplitude activity.

C. High anesthetic drug concentration (about 2 MAC)

We have determined the equilibrium solution of h_e and studied their linear stability when anesthetic drug concentration is varied between 0 and 1.8 mM. Figure 11 displays the results where stars and circles correspond to stable and unstable solutions, respectively. For a wide range of anesthetic drug concentration, simulated EEG signals have almost the same morphologies. Therefore, we select a candidate concentration value within this range to examine the behavior of the model. Figure 5(d) represents s, h_e isoclines corresponding to $c=1.5$ mM. The intersection of the two isoclines occurs in middle branch of h_e isocline. Linear stability analysis shows that the model has a unique equilibrium point which is unstable.

The time course and power spectrum of the numerically simulated h_e signal in Figs. 6(d) and 7(d) show that the rate of negative peaks in $h_e(t)$ is more or less similar to what we had for $c=0.9$ mM and it is higher than what we had for $c=0.75$ mM. Figure 6(d) also shows that the switching between up and down states is more regular. This can also be testified by means of the histogram of h_e fluctuations, which depicts two dominant peaks.

Figure 9(d) illustrates a real EEG signal at 2 MAC [37]. Visually inspection of this figure shows that our model is still able to generate signals miming real EEG recordings. The power spectrum of the EEG signal, basically consists of a semiperiodic 2.3 Hz activity. Due to this semiperiodic activity, the power of the fast delta band (e.g., 2–4 Hz) may even become greater than the power of the slow delta band (e.g., 0–2 Hz) at 2 MAC [42]. Similar behavior is expressed by simulated data [see Fig. 7(d)].

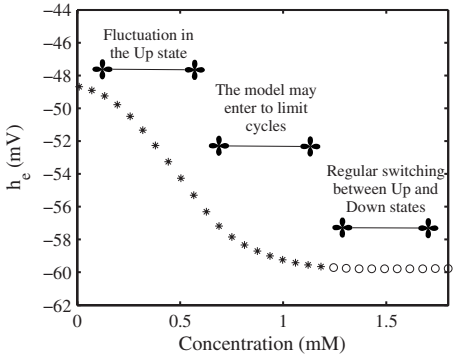

FIG. 11. Equilibrium solutions of h_e when anesthetic drug concentration is varied between 0 and 1.8 mM. Stars are stable and circles are unstable solutions of linear stability analysis.

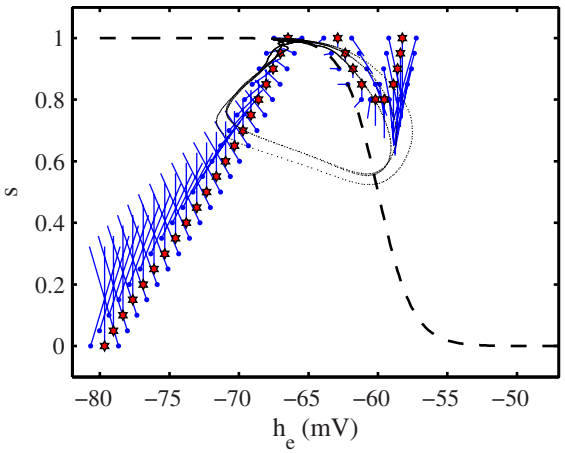

FIG. 12. (Color online) s,h_e isoclines and a 20 s (s,h_e) trajectory corresponding to burst suppression in high anesthetic drug concentration ($c=1.8$, $B=0.14$, $\theta_s=-60$). The intersection of the two isoclines is very close to the saddle point of the h_e isocline so (s,h_e) trajectory has the possibility of short-time traveling from down to up state.

D. Burst-suppression

EEG suppression is the last phenomenon to be observed in very deep anesthesia. About 30% of EEG signals in the Tirel *et al.* experiment [37], exhibit suppressed activity at 2 MAC Desflurane anesthesia. Sometimes EEG suppressions alternate with bursting activities. This phenomenon is the so-called burst-suppression pattern. Bursts result from short-time discharges of single cells action potentials. Although the enhanced model was not optimized for simulating burst-suppression patterns, it is able to qualitatively reproduce EEG dynamics showing bursting activities and the transition toward full suppression.

A burst is generated when neural cells jump temporarily from down to up state. The enhanced model can reproduce such activity if s,h_e isoclines intersect in the down state area in the vicinity of the unstable middle branch of h_e isocline. For example, if we keep all parameters of the model constant but reduce the modulation strength of the slow mechanism slightly (e.g., $B=0.14$, $\theta_s=-60$), burst suppression is generated. Figure 12 shows the two isoclines of the model when drug concentration is 1.8 mM. The intersection of the two isoclines is very close to the saddle point of the h_e isocline so (s,h_e) trajectory that is generally located in the vicinity of the down state equilibrium point, may sometimes switch to the up state for short periods. Figure 13 shows $h_e(t)$ corresponding to the illustrated trajectory in Fig. 12. The histogram of h_e, which only consists of a single peak in the down state area is depicted in Fig. 14.

By decreasing the drug concentration, h_e isocline moves toward the negative direction of the s axis so the equilibrium point becomes closer to the middle branch of h_e isocline (unstable area). Consequently, (s,h_e) trajectory may escape from the down state area easier than before. This increases the number of bursts on the EEG signal, which is in agreement with Bruhn's experiments [43,44]. On the other hand, increasing the drug concentration or blocking the slow modulating mechanisms reduces the possibility of burst generation. In such a case the model may remain in a suppressed mode if subcortical inputs do not activate the model by triggering events.

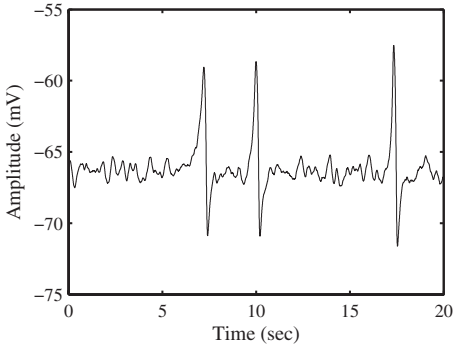

FIG. 13. Twenty seconds of simulated h_e signal corresponding to the illustrated (s,h_e) trajectory in Fig. 12. This activity is reminiscent of burst-suppression activity in deep anesthesia.

VI. DISCUSSIONS AND CONCLUSIONS

Modeling is unavoidably based on simplifications of real systems. In our viewpoint, the simpler the model that can explain a particular phenomenon, the more fundamental is its scope. The proposed MF model encompasses the two most important neural populations in the neocortex (pyramidal and interneurons) and a slow mechanism that modulates the firing rate of pyramidal population. It is an easy to understand model by which we can study the role of inhibitory and excitatory factors as well as the slow modulating mechanism of the excitatory firing rate in various anesthetic concentrations.

Since internal states of a neural network and single neurons are closely related to each other, a population of neural cells may exhibit bursts of activity (like single neurons) even if it has been settled in down state. Without including any modulating parameter in the model, a static form of the sigmoid relationship between the mean membrane potential and the firing rate does not justify the generation of bursts in very

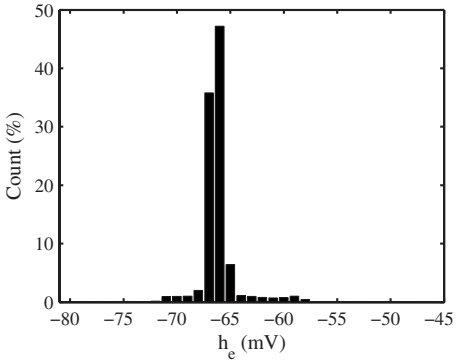

FIG. 14. The histogram of the depicted signal in Fig. 13. The histogram only has one peak in the down state area.

low potentials. We redefined the sigmoid relationship and included the influence of a typical slow modulating mechanism. Out of various types of modulating parameters that may modulate the mean firing rate of a neural population, we only considered a generic slow voltage-dependent ionic current. It should be remembered that there are many kinds of modulating mechanisms in the brain and each mechanism may have its own characteristics (e.g., different time constants) and may exhibit different behaviors in different anesthetic drug concentrations. In this model, the overall effects of all types of slow mechanisms have been gathered in a voltage-dependent mechanism leading to a new functioning mode (i.e., up and down states), which better explains the occurrence of high amplitude slow waves in the EEG. However, in order to further improve the model, MF characteristics of the most important modulating mechanisms in cortical and subcortical areas should be identified and incorporated.

Compared to previous MF models, the working modes of the enhanced model are closer to some neurophysiological observations. For example, experimental results show that in an overall view, neural cell activities may be classified as continuous, phasic, or silence. The single point equilibrium solution of the model in each drug concentration (Fig. 11) is in accordance with this classification. If this single point equilibrium solution is stable, it represents either a high firing-rate continuous activity (up state) or silence (down state). If the equilibrium solution is unstable or very close to the unstable region, it corresponds to switching of neural activities between the two states.

Nonsmooth variation of stable equilibrium solutions [7,8] is not in agreement with a smooth reduction of neural firing rates with anesthetic drug concentration [26]. A single stable branch in various drug concentrations [9] does not justify the two different firing states of neural populations (e.g., in slow waves or burst suppression). On the contrary, equilibrium solutions of the enhanced model vary smoothly in a dose-dependant manner from up to down state. This model considers the two firing states of neural populations so it can reproduce some internal states of neural populations [23] such as continuous activities in up state, transient jumps from up to down state, regular switching between up and down states, burst suppression, and suppression. In general, the maximum firing rate value of a neural population does not change noticeably before and after applying an anesthetic agent [26]. The mean firing rate value of a neural population is mainly reduced by the occurrence of a silence phase between firing phases [16]. Firing patterns of neural populations of the enhanced model (see Fig. 15) are in agreement with these remarks, while in previous MF models, mean and maximum firing rate values are jointly reduced by increasing anesthetic concentration.

In the enhanced model, the sudden transition between awareness and unconsciousness may be interpreted by sudden transition between internal states of neural populations induced by similar behaviors in single neurons [23]. According to different activity modes represented in Sec. V, it is probable that awareness and unconsciousness are two disjoint mental states because firing patterns of neural populations are changed suddenly from continuous mode to phasic mode as if the information processing mode of the brain is changed suddenly by administrating an anesthetic agent. Such a result needs to be confirmed by experimental data showing the evolution of neural membrane potentials and firing rates during the awareness-unconsciousness transition.

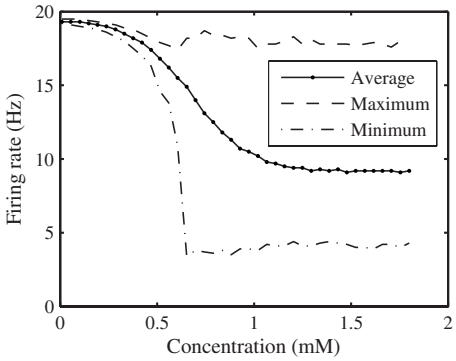

FIG. 15. Average and extremum values of the excitatory firing rate in different drug concentrations. Firing rates are calculated based on numerical simulation of the model for 51.2 s.

The enhanced model also has some limitations. A single homogeneous neocortical module is introduced without considering other parts of the brain such as the thalamus and hippocampus; therefore, it is not forced to reproduce some typical EEG activities such as spindles and alpha rhythm that are generated in these parts of the brain. It has been suggested that spindles are generated in the thalamus [45] and corticothalamic inputs control the patterns of activities in the thalamus and thalamocortical networks [46,47]. Recent studies show that a distributed alpha network, which consists of thalamus, cortex, and hippocampus is engaged in alpha oscillations. A communication exists between neocortex and hippocampus during alpha oscillations [48] and hippocampus can react to sensory stimuli with a 10 Hz enhancement [49].

In future studies, a model aimed at generating slow and delta rhythms as well as spindles and alpha rhythm will be built by integrating underlying synaptic and ionic mechanisms located in cortical and subcortical regions. It would be useful also to expand the enhanced model to a nonhomogenous one.

It should be emphasized that in a stable situation, the amplitude of the simulated EEG signal (h_e) is mainly determined by the variance of input noises and characteristics of the transfer function of the model, but in an unstable situation (limit cycle), it is mainly determined by the potential difference between the left and right branches of h_e isocline (i.e., up and down states). However, because of individual dissimilarities in the structures of different single neural cells, they may switch to up and down state not in a fully synchronized manner. According to our EEG recordings on children (Fig. 9) and Constant *et al.* experiments [50] it can be inferred that the amplitude ratio is almost equal to 10 before and after administration of anesthetics. The amplitude ratio of reproduced EEG signals (Fig. 6) is comparable with the empirical amplitude ratio in children, but it is higher than the amplitude ratio in adults [51]. It has been stated that this amplitude ratio is decreased by the age and maturation of neural cells [50,51]. Such an increase in amplitude ratio is

also observed in reproduced K-complexes in the Wilson *et al.* model [52]. The amplitude ratio of K-complexes to background EEG activities in this model is slightly higher than the one in empirical data [19]. It seems that maturation of neural cells or, equivalently, specialization of neural cells to do more specific tasks in the brain induces less similarity between them. As a result, synchronization between adjacent neural cells in a local field is higher for children than for adults.

One of the basic assumptions in designing population equations is that neural cells are identical and have similar properties in a volume of one macrocolumn. Prominent examples are columns in the somatosensory and visual cortex and pools of motor neurons. Dissimilarities in structure and the function of neural cells in a local field degrade the above assumption; so it seems that maturation of neural cells and their potency of synchronization are still required to be considered somehow (for example, by dividing inhibitory and excitatory populations into some subpopulations and randomizing their parameters) in MF models. This may fill the gap which exists between full-synchronous and asynchronous activities.

At last, we want to mention that *biphasic* is a transient dynamic response of the brain which, is basically originated from fast variations of brain inputs (e.g., drug concentration) during the time. It is shown that changing the speed of the administration of an anesthetic drug changes the characteristics of biphasic response and the concentration in which the maximum of the biphasic response appears [15]. In general, at a given drug concentration, EEG amplitudes are not identical in steady-state and transient conditions. Behavior of our enhanced MF model is discussed in steady-state condition so a simulated EEG signal in this condition should be compared with a real EEG signal recorded in steady-state condition not in transient condition.

ACKNOWLEDGMENT

This work was partly financed by the French Ministry of Research and Technology (Grant No. DT 03 B 107-108-109; CITH Rennes).

APPENDIX

This Appendix briefly describes the basic equations of the enhanced MF model that were derived from the pioneering works of Steyn-Ross *et al.* [6–8] and Bojak and Liley [9]. Since these equations are now well covered in many other journals, we do not define them in so much detail. For definitions of the parameters of the model see Table I.

Equation (A1) depicts the two main differential equations of the model that express mean membrane potentials of inhibitory and excitatory populations (h_e, h_i).

$$\tau_k \frac{dh_k(t)}{dt} = h_k^{\text{rest}} - h_k + \psi_{ek}(h_k) I_{ek}(h_e) + \psi_{ik}(h_k) I_{ik}(h_i), \quad k = \{e,i\}, \tag{A1}$$

$$\psi_{jk}(h_k) = [h_j^{\text{rev}} - h_k]/|h_j^{\text{rev}} - h_k^{\text{rest}}|. \tag{A2}$$

j and k may represent either excitatory (e) or inhibitory (i). ψ_{jk} is a scaling factor and indicates the potency of synapses between j- and k-type populations. I_{jk} represents voltaic influences of synapses and is represented in Eq. (A3) by convolving the firing rate of k population and j-type postsynaptic potential (PSP) function. The bracketed term in the right hand side of Eq. (A3) represents the firing rate of k-type population, which is composed of three sources: locally in the same macrocolumn (S_j), distant from other macrocolumns (Φ_{jk}), and subcortical inputs (p_{jk}).

$$\left(\frac{d}{dt} + \gamma_j\right)\left(\frac{d}{dt} + \bar{\gamma}_j\right) I_{jk}(t) = [N_{jk}^{\beta} S_j(h_j) + \Phi_{jk} + p_{jk}] \times G_j \bar{\gamma}_j e^{\gamma_j \delta_j(\gamma_j, \bar{\gamma}_j)}, \quad j,k = \{e,i\}. \tag{A3}$$

PSPs are represented by biexponential functions. G_j, γ_j, and $\bar{\gamma}_j$ determine maximum values, rising and falling time constants of the biexponential functions. These parameters are varied by anesthetic drug concentrations. Instead of directly applying the influence of anesthetic drugs on γ_j and $\bar{\gamma}_j$, it is more convenient to define two alternative parameters (δ_j and ζ_j) and then modify them by drug concentration [9]. δ_j is the time lag of PSP maximum peak and ζ_j is the decay time of PSP function.

S_j determines the mean firing rate of j-type population from mean membrane potential. A sigmoid function is employed to represent this relationship [53].

$$S_j(h_j) = S_j^{\max}/\{1 + \exp[-g_j(h_j - \theta_j)]\}, \tag{A4}$$

where $S_j^{\max}$ denotes the maximum firing rate; θ_j and g_j, respectively, determine the inflection point and its slope in the sigmoid function.

Distant generated firing rates (Φ_{jk}) are only confined to excitatory originated because the long-distance coupling from inhibitory populations is unlikely ($\Phi_{ik}=0$). Φ_{ek} is determined by applying a spatial-temporal filter on $S_e(h_e)$. Since the brain has been assumed to be a homogeneous media no spatial variable is seen in Eq. (A5).

$$\left(\frac{d}{dt} + \bar{v}\Lambda_{ek}\right)^2 \Phi_{ek}(t) = \bar{v}^2 \Lambda_{ek}^2 N_{ek}^{\alpha} S_e(h_e). \tag{A5}$$

For simplicity, each subcortical noise is modeled by Eq. (A6). However, it should be mentioned that there are also other formulations for representations of subcortical noises [9,54] that may be employed in more specialized studies according to their specific purposes. In Eq. (A6), $\bar{p}_{jk}$ is a constant value and represents the incoming mean firing rate of the j-type subcortical population to k-type cortical population. $\xi_{jk}(t)$ is a zero mean uniform white noise that extends between -1 and $+1$, so the variance of $\bar{p}_{jk}$ is equal to $\alpha^2 \bar{p}_{jk}^2/3$. α is a scaling factor that controls the variance of the noises and can be used to prevent the generation of negative value noises in numerical simulations.

$$p_{jk}(t) = \bar{p}_{jk} + \alpha \bar{p}_{jk} \xi_{jk}(t). \quad \text{(A6)}$$

Administration of anesthetic drugs changes the shape of PSPs. Based on real experimental data it is possible to relate the amplitude and time constant of IPSP or EPSP to different anesthetic drug concentrations. We used the following Hill equations (for more discussion see Refs. [9,55]) to express variations of maximum amplitudes and decay times of IPSPs and EPSPs in different concentrations of a generic anesthetic drug as follows:

$$G_j(c_{\mathrm{MAC}}) = G_j^0 \frac{K_j^{N_j} + M_j c_{\mathrm{MAC}}^{N_j}}{K_j^{N_j} + c_{\mathrm{MAC}}^{N_j}}, \quad j = \{i,e\}, \quad \text{(A7)}$$

$$\zeta_i(c_{\mathrm{MAC}}) = \zeta_i^0 \frac{k_i^{n_i} + m_i c_{\mathrm{MAC}}^{n_i}}{k_i^{n_i} + c_{\mathrm{MAC}}^{n_i}}, \quad \zeta_e(c_{\mathrm{MAC}}) = \zeta_e^0, \quad \text{(A8)}$$

where c_{MAC} is the alveolar drug concentration in MAC (1 MAC is the minimum alveolar concentration of an anesthetic agent at 1 atmosphere pressure at which 50% of patients still move in response to a noxious stimulus). K_i, M_i, N_i, K_e, M_e, N_e, k_i, m_i, and n_i are free parameters of Hill equations that have been assigned with 1.25, 0.37, 2.3, 2.5, 0.5, 1, 0.975, 4.4, and 2.8, respectively, for our generic anesthetic drug. G_j^0 and ζ_j^0 are the maximum amplitude and decay time of j-type PSP at zero drug concentration.

In this paper we use 1 MAC=8.3 vol % for Desflurane. This is appropriate for young children [38] and corresponds to $c_{\mathrm{aq}} \simeq 0.73$ mM aqueous concentration of Desflurane in saline [39,40] considering that the saline or gas partition coefficient is equal to 0.225 for Desflurane [56].

To express Eqs. (A7) and (A8) as functions of aqueous concentration of Desflurane (c_{aq}) or vol % (c_{vol}), it is only necessary to replace K_j and k_i with μK_j and μk_i, where μ is equal to 0.73 and 8.3 for c_{aq} and c_{vol}, respectively. In this study, we express the concentration of Desflurane (c) by its aqueous concentration c_{aq}.

[1] L. Senhadji, E. Wodey, and E. Claude, Crit. Rev. Biomed. Eng. **30**, 85 (2002).
[2] W. Gerstner and W. M. Kistler, *Spiking Neuron Models: Single Neurons, Populations, Plasticity* (Cambridge University Press, Cambridge, England, 2002).
[3] A. Renart, N. Brunel, and X. J. Wang, in *Computational Neuroscience: A Comprehensive Approach*, edited by J. Feng (CRC Press, Boca Raton, 2003), p. 431.
[4] D. T. J. Liley, P. J. Cadusch, and J. J. Wright, Neurocomputing **26-27**, 795 (1999).
[5] D. T. Liley, P. J. Cadusch, and M. P. Dafilis, Network **13**, 67 (2002).
[6] M. L. Steyn-Ross, D. A. Steyn-Ross, and J. W. Sleigh, Prog. Biophys. Mol. Biol. **85**, 369 (2004).
[7] M. L. Steyn-Ross, D. A. Steyn-Ross, J. W. Sleigh, and L. C. Wilcocks, Phys. Rev. E **64**, 011917 (2001).
[8] D. A. Steyn-Ross, M. L. Steyn-Ross, L. C. Wilcocks, and J. W. Sleigh, Phys. Rev. E **64**, 011918 (2001).
[9] I. Bojak and D. T. Liley, Phys. Rev. E **71**, 041902 (2005).
[10] T. G. Weyand, M. Boudreaux, and W. Guido, J. Neurophysiol. **85**, 1107 (2001).
[11] M. Steriade, I. Timofeev, and F. Grenier, J. Neurophysiol. **85**, 1969 (2001).
[12] A. Compte, M. V. Sanchez-Vives, D. A. McCormick and X. J. Wang, J. Neurophysiol. **89**, 2707 (2003).
[13] M. Massimini and F. Amzica, J. Neurophysiol. **85**, 1346 (2001).
[14] M. Bazhenov, I. Timofeev, M. Steriade and T. J. Sejnowsk, J. Neurosci. **22**, 8691 (2002).
[15] K. Kuizenga J. H. Proost, J. M. Wierda, and C. J. Kalkman, Anesthesiology **95**, 607 (2001).
[16] B. Antkowiak and D. Heck, J. Neurophysiol. **77**, 2525 (1997).
[17] B. Antkowiak and C. Helfrich-Forster, Anesthesiology **88**, 1592 (1998).
[18] D. Pare, E. Shink, H. Gaudreau, A. Destexhe and E. J. Lang , J. Neurophysiol. **79**, 1450 (1998).
[19] F. Amzica and M. Steriade, Sleep Medicine Reviews **6**, 139 (2002).
[20] C. Bedard, H. Kroger, and A. Destexhe, Biophys. J. **86**, 1829 (2004).
[21] M. Rudolph, J. G. Pelletier, D. Pare, and A. Destexhe, J. Neurophysiol. **94**, 2805 (2005).
[22] A. Destexhe, M. Rudolph, J. M. Fellous, and T. J. Sejnowski, Neuroscience **107**, 13 (2001).
[23] S. Fujisawa, N. Matsuki, and Y. Ikegaya, Cereb. Cortex **16**, 639 (2006).
[24] B. Antkowiak, H. Hentschke, and K. Kirschfeld, Br. J. Anaesth. **79**, 617 (1997).
[25] K. Nishikawa and M. B. Maclver, Anesthesiology **94**, 340 (2001).
[26] B. Antkowiak, Anesthesiology **91**, 500 (1999).
[27] B. Antkowiak, Naturwiss. **88**, 201 (2001).
[28] P. G. Barash, B. F. Cullen, and R. K. Stoetting, in *Clinical Anesthesia* Lippincott Williams and Wilkins, Philadelphia (2005), p. 111.
[29] D. Bleakman, M. V. Jones, and N. L. Harrison, Neuropharmacology **34**, 541 (1995).
[30] C. R. Ries and E. Puil, J. Neurophysiol. **81**, 1802 (1999).
[31] C. R. Ries and E. Puil, J. Neurophysiol. **81**, 1795 (1999).
[32] I. Timofeev and M. Steriade, J. Neurophysiol. **76**, 4152 (1996).
[33] F. Kasanetz, L. A. Riquelme, and M. G. Murer, J. Physiol. (London) **543**, 577 (2002).
[34] I. Timofeev, F. Grenier, M. Bazhenov, T. J. Sejnowski, and M. Steriade, Cereb. Cortex **10**, 1185 (2000).
[35] M. Steriade, A. Nunez, and F. Amzica, J. Neurosci. **13**, 3266 (1993).
[36] M. Steriade, R. C. Dossi, and A. Nunez, J. Neurosci. **11**, 3200 (1991).
[37] O. Tirel, E. Wodey, R. Harris, J. Y. Bansard, C. Ecoffey, and L. Senhadji, Br. J. Anaesth. **96**, 480 (2006).
[38] W. W. Mapleson, Br. J. Anaesth. **76**, 179 (1996).

[39] N. P. Franks and W. R. Lieb, Br. J. Anaesth. **71**, 65 (1993).
[40] N. P. Franks and W. R. Lieb, Anesthesiology **84**, 716 (1996).
[41] N. Brunel and X.-J. Wang, J. Neurophysiol. **90**, 415 (2003).
[42] B. Molaee Ardekani, M. B. Shamsollahi, L. Senhadji, E. Wodey and B. Vosoughi Vahdat in *World Congress on Medical Physics and Biomedical Engineering WC2006*, edited by S. I. Kim and T. S. Suh (Springer, Berlin, Heidelberg, New York, Seoul-Korea, 2006).
[43] J. Bruhn, H. Ropcke, B. Rehberg, T. Bouillon, and A. Hoeft, Anesthesiology **93**, 981 (2000).
[44] J. Bruhn, T. W. Bouillon, and S. L. Shafer, J. Clin. Monit Comput. **16**, 593 (2000).
[45] M. Steriade, L. Domich, G. Oakson, and M. Deschenes, J. Neurophysiol. **57**, 260 (1987).
[46] H. Blumenfeld and D. A. McCormick, J. Neurosci. **20**, 5153 (2000).
[47] A. Destexhe, D. Contreras, and M. Steriade, Neuroscience **92**, 427 (1999).
[48] A. Sirota, J. Csicsvari, D. Buhl, and G. Buzsaki, Proc. Natl. Acad. Sci. U.S.A. **100**, 2065 (2003).
[49] M. Schurmann, T. Demiralp, E. Basar, and C. Basar Eroglu, Neurosci. Lett. **292**, 175 (2000).
[50] I. Constant, R. Seeman, and I. Murat, Paediatr. Anaesth. **15**, 266 (2005).
[51] A. Schultz, U. Grouven, I. Zander, F. A. Beger, M. Siedenberg, and B. Schultz, Acta Anaesthesiol. Scand. **48**, 27 (2004).
[52] M. T. Wilson, D. A. Steyn-Ross, J. W. Sleigh, M. L. Steyn-Ross, L. C. Wilcocks, and I. P. Gillies, J. Comput. Neurosci. **21**, 243 (2006).
[53] H. R. Wilson and J. D. Cowan, Biophys. J. **12**, 1 (1972).
[54] G. D. Smith, C. L. Cox, S. M. Sherman, and J. Rinzel, Thalamus and Related Systems **1**, 135 (2001).
[55] D. T. Liley and I. Bojak, J. Clin. Neurophysiol. **22**, 300 (2005).
[56] E. I. Eger, II, Anesth. Analg. (Baltimore) **66**, 971 (1987).